INT. J. REMOTE SENSING, 20 DECEMBER, 2003,
VOL. 24, NO. 24, 5161–5182

Taylor & Francis
Taylor & Francis Group

Surface temperature and water vapour retrieval from MODIS data

J. A. SOBRINO, J. EL KHARRAZ

Department of Thermodynamics, Faculty of Physics, University of Valencia, 50 Dr. Moliner, 46100, Burjassot, Spain; e-amil: sobrino@uv.es; jauad@uv.es

and Z.-L. LI

Temps Réel et InterOpérabilité, Laboratoire des Sciences de l'Image, de l'Informatique, et de la Télédétection (TRIO/LSIIT) Centre Nationale de la Recherche Scientifique, Unité Mixte de Recherche (CNRS UMR 7005), 5 Boulevard Sebastien Brant, 67400 Illkirch, France; e-mail: Li@sepia.u-strasbg.fr

(*Received 14 May 2002; in final form 10 February 2003*)

Abstract. This paper gives operational algorithms for retrieving sea (SST), land surface temperature (LST) and total atmospheric water vapour content (W) using Moderate Resolution Imaging Spectroradiometer (MODIS) data. To this end, the MODTRAN 3.5 radiative transfer program was used to predict radiances for MODIS channels 31, 32, 2, 17, 18 and 19. To analyse atmospheric effects, a simulation with a set of radiosonde observations was used to cover the variability of surface temperature and water vapour concentration on a worldwide scale. These simulated data were split into two sets (DB1 and DB2), the first one (DB1) was used to fit the coefficients of the algorithms, while the second one (DB2) was used to test the fitted coefficients. The results show that the algorithms are capable of producing SST and LST with a standard deviation of 0.3 K and 0.7 K if the satellite data are error free. The LST product has been validated with *in situ* data from a field campaign carried out in the Mississippi (USA), the results show for the LST algorithm proposed a root mean square error lower than 0.5 K. Regarding water vapour content, a ratio technique is proposed, which is capable of estimating W from the absorbing channels at 0.905, 0.936, and 0.94 μm, and the atmospheric window channel at 0.865 μm, with a standard deviation (in the comparison with radiosonde observations) of 0.4 g cm^{-2}.

1. Introduction

One of the most important parameters in all surface–atmosphere interactions and energy fluxes between the ground and the atmosphere is land surface temperature (LST). It is also a good indicator of the energy balance at the Earth's surface (Sellers *et al.* 1988). As such, LST is used as a parameter for a wide variety of scientific studies and agricultural applications (e.g. Caselles and Sobrino 1989, Vining and Blad 1992, Kimura and Shimura 1994). Because of the difficulties in correcting for atmospheric absorption, atmospheric emission and surface emissivity

International Journal of Remote Sensing
ISSN 0143-1161 print/ISSN 1366-5901 online
http://www.tandf.co.uk/journals
DOI: 10.1080/0143116031000102502

(Watts *et al.* 1996), the development of accurate LST algorithms is not an easy task. On the other hand, the knowledge of the total amount of atmospheric water vapour helps in the development of accurate LST algorithms and moreover is an important parameter to understand the hydrological cycle, biosphere–atmosphere interaction, and the energy budget, as well as to monitor climate change due to greenhouse gases.

Experience in retrieving sea surface temperature (SST), LST and total atmospheric water vapour content (W) has been carried out using sensors such as the Along-Track Scanning Radiometer (ATSR), the Advanced Very High Resolution Radiometer (AVHRR) (Sobrino *et al.* 1999), and the Moderate Resolution Imaging Spectroradiometer (MODIS) (Wan and Dozier 1996, Wan and Li 1997, Brown and Minnett 1999). In this paper, our objective is to propose operational algorithms to retrieve LST and total atmospheric water vapour content from MODIS data. This sensor on board NASA's EOS AM-1 (Earth Observing System) TERRA satellite, was successfully launched from Vandenberg Air Force Base (VAFB) in Lompoc, California, on 18 December 1999. The MODIS Instrument views the entire Earth's surface every 1 to 2 days, with instantaneous fields-of-view (IFOVs) of 250 m (channels 1–2), 500 m (channels 3–7), and 1 km (channels 8–36) and a scan angle of $+/-$ 55° from nadir, acquiring data in 36 spectral channels, 16 being in the thermal infrared (TIR) from 3–15 μm. The performance of the MODIS instrument may be affected by any potential small change in the optical status of the instrument caused in the rapid launch process and in the long period of post-launch instrument outgases in the orbit. On the other hand, it is important to have knowledge of the systematic error and noise in the MODIS level-1B radiance data (Version 2.3.x) (Guenther *et al.* 1998) before evaluating the calibration accuracy and the use of MODIS TIR data. Wan (2002), has estimated the noise and the systematic error in early MODIS TIR data and concluded that systematic error is small in bands 31 and 32, which are used to obtain LST in the present work.

2. Land surface temperature

2.1. *Theory*

For a cloud-free atmosphere under local thermodynamic equilibrium, the radiative transfer equation gives the radiance $I_{i\theta}$ measured from space in channel i under zenith observation angle θ as the sum of three terms: (1) the radiation emitted by the surface that is attenuated by the atmosphere, (2) the upwelling radiation emitted by the atmosphere towards the sensor, and (3) the downwelling radiation emitted by the atmosphere that reaches the Earth's surface and is then reflected towards the sensor:

$$I_{i\theta} = B_i(T_{i\theta}) = \varepsilon_{i\theta} B_i(T_s)\tau_{i\theta} + R_{ati\theta\uparrow} + R_i(\text{ref})\tau_{i\theta} \tag{1}$$

where all quantities refer to a spectral integration over the band width of channel i, B_i is Planck's function, $T_{i\theta}$ is the brightness temperature measured at satellite level at zenith observation angle θ, $\varepsilon_{i\theta}$ is the ground surface emissivity at zenith angle θ, $\mathrm{B_i}(T_s)$ is the radiance that would be measured if the surface were a blackbody with the surface temperature T_s, $\tau_{i\theta}$ is the total atmospheric path transmittance at zenith angle θ, $R_{ati\theta\uparrow}$ is the atmospheric upwelling radiance at the zenith angle θ, which is

given as:

$$R_{ati\theta\uparrow} = (1-\tau_{i\theta})B_i(T_a) \tag{2}$$

where T_a represents a mean temperature of the atmosphere between the surface and the highest level where the information comes from (i.e. the top of atmosphere), and R_i(ref) is the reflected atmospheric radiance, which is given as:

$$R_i(\text{ref}) = (1-\varepsilon_{i\theta})(1-\tau_{i53})B_i(T_a) \tag{3}$$

where τ_{i53} is the total atmospheric path transmittance at zenith angle 53°. In this way, substituting (2) and (3) in (1), making a linearization of the Planck function and writing the resulting equation for two channels i and j, Sobrino *et al.* (1996) arrived at the following expression for the split-window method:

$$T_s = T_i + A\left(T_i - T_j\right) - B_0 + (1-\varepsilon)B_1 - \Delta\varepsilon B_2 \tag{4}$$

where A, B_0, B_1 and B_2 are the split-window coefficients given by:

$$A = (1-\tau_i)/\left(\tau_i - \tau_j\right) \tag{5}$$

$$B_0 = \left(1-\tau_j\right)\left(T_{ai} - T_{aj}\right) \tag{6}$$

$$B_1 = \left[(1-\tau_i\tau_{i53})/\left(\tau_i - \tau_j\right)\right]\left(T_i - T_j\right) + \tau_{i53}L_i \tag{7}$$

$$B_2 = \tau_j A\ B_1 \tag{8}$$

where T_i and T_j are the brightness temperatures measured in two different MODIS channels, $\varepsilon = (\varepsilon_i + \varepsilon_j)/2$, $\Delta\varepsilon = \varepsilon_i - \varepsilon_j$, L_i is a parameter with dimension of temperature, and T_{ai} and T_{aj} are respectively, the mean atmospheric temperatures of channels i and j. In this way, equation (4) permits a separation between the atmospheric and emissivity effects in the retrieval of surface temperature.

2.2. *Simulation of satellite measurements*

Simulations of satellite measurements of SST and LST have been carried out. The MODTRAN 3.5 radiative transfer program (Abreu and Anderson 1996) was used to simulate MODIS data. MODTRAN 3.5 includes all the functional capabilities of LOWTRAN 7 (Low Resolution Transmittance Code) (Kneizys *et al.* 1988), but uses a more accurate and higher resolution molecular band model with $2\,\text{cm}^{-1}$ resolution based on the HITRAN (Atlas of High Resolution Molecular Spectroscopic Data) molecular database (Rothman *et al.* 1992). MODTRAN calculations typically agree to within 0.5 K in comparison with detailed line-by-line (LBL) models (Soden *et al.* 2000). The MODTRAN 3.5 provides atmospheric profiles (temperature, pressure, water vapour density, ozone density, and aerosol density) for six standard atmospheres: US standard, mid-latitude summer, mid-latitude winter, subarctic summer, subarctic winter, and tropical. It is possible using this radiative transfer program to predict the radiances for MODIS infrared channels at the satellite altitude (705 km) with the appropriate channel filter functions (see figure 1 and table 1).

In order to analyse atmospheric effects a set of two radiosonde observation databases were extracted carefully from the TOVS Initial Guess Retrieval (TIGR) database (Chesters *et al.* 1983): 61 radiosonde observations (DB1) to determine the split window coefficients, and 183 radiosonde observations (DB2) (figure 2) to test the coefficients, both of them covering the variability of surface temperature from

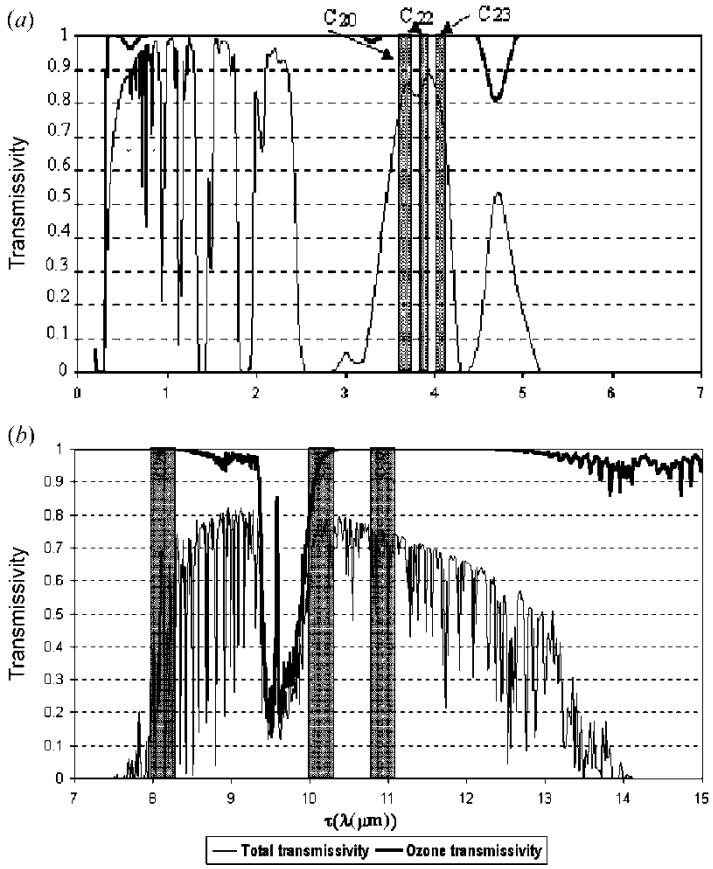

Figure 1. Total atmospheric and ozone transmissivities for MODIS channels given in table 1 as a function of wavelength. The values have been obtained for a tropical atmosphere at nadir.

Table 1. Spectral characteristics of MODIS thermal channels.

Band number	Band centre (μm)	Bandwidth (μm)	NEΔT (K)
20	3.75	0.18	0.05
22	3.959	0.06	0.07
23	4.05	0.06	0.07
29	8.55	0.3	0.05
31	11.03	0.5	0.05
32	12.02	0.5	0.05

230 to 330 K, and water vapour concentration from 0.09 to 6.37 g cm^{-2} on a worldwide scale. The attenuation of the surface radiance has been considered by adding the uniformly mixed gases (CO_2, N_2O, O_3, CO and CH_4), included in the standard atmospheres of the MODTRAN 3.5 program, to the water vapour taken from profiles in TIGR radiosonde observations. Figure 3 shows atmospheric

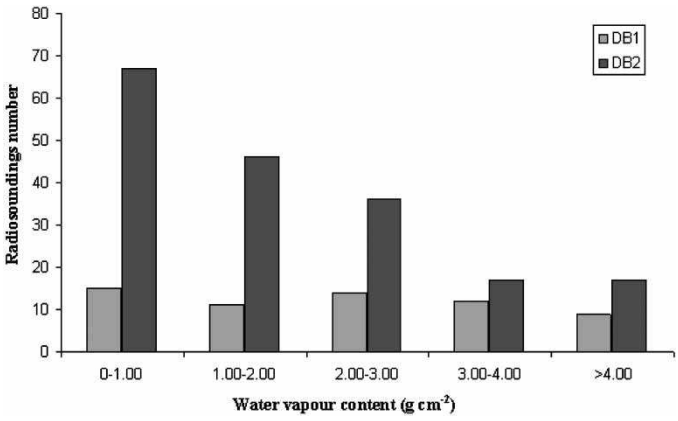

Figure 2. Histogram of the total atmospheric water vapour content of the two databases considered (DB1) and (DB2).

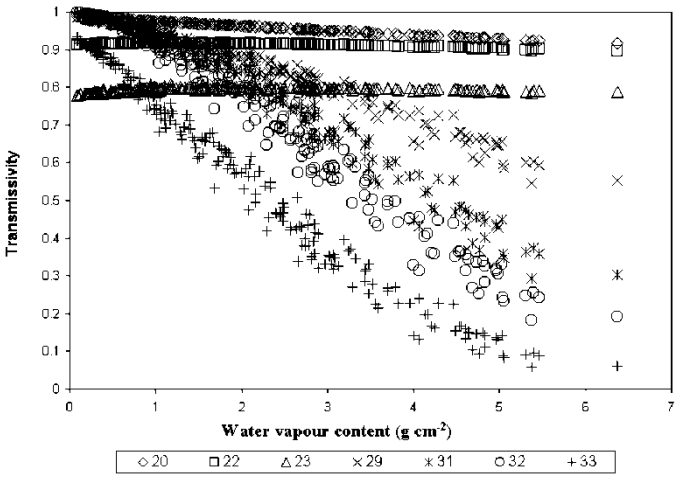

Figure 3. Atmospheric transmittances for MODIS channels 20, 22, 23, 29, 31 and 32 as a function of the total atmospheric water vapour content at nadir, W. The values have been obtained for all the radiosonde observations.

transmittances of the MODIS channels 20, 22, 23, 29, 31 and 32 at nadir for the database considered. The figure clearly shows the strong decrease of the transmittances with total atmospheric water vapour content for channels 29, 31 and 32, while for channels 20, 22 and 23 the transmittances are nearly independent of water vapour content.

In order to include a wide range of variability in the atmospheric and surface conditions, we have considered in the simulation for each atmospheric profile three observation angles: 0°, 32°, 50°, five surface temperatures ($T-5$, T, $T+5$, $T+10$,

Table 2. Terrestrial materials used in the simulation. Sample nomenclature has been taken from Salisbury and D'Aria (1992).

Rocks				
Igneous	Sedimentary	Soils	Vegetation	Water
Desert vanish coated rock	Suspended sediments (qtzwater)	Ultisols 0145	Green foliage	Distwater/ sea water
Lichen coated rock	Sandstone	Vertisols 0475	Decomposing litter	Ice
Metamorphic rock	Shale	Aridisols1530		
	Siltstone	Oxisols 4717		

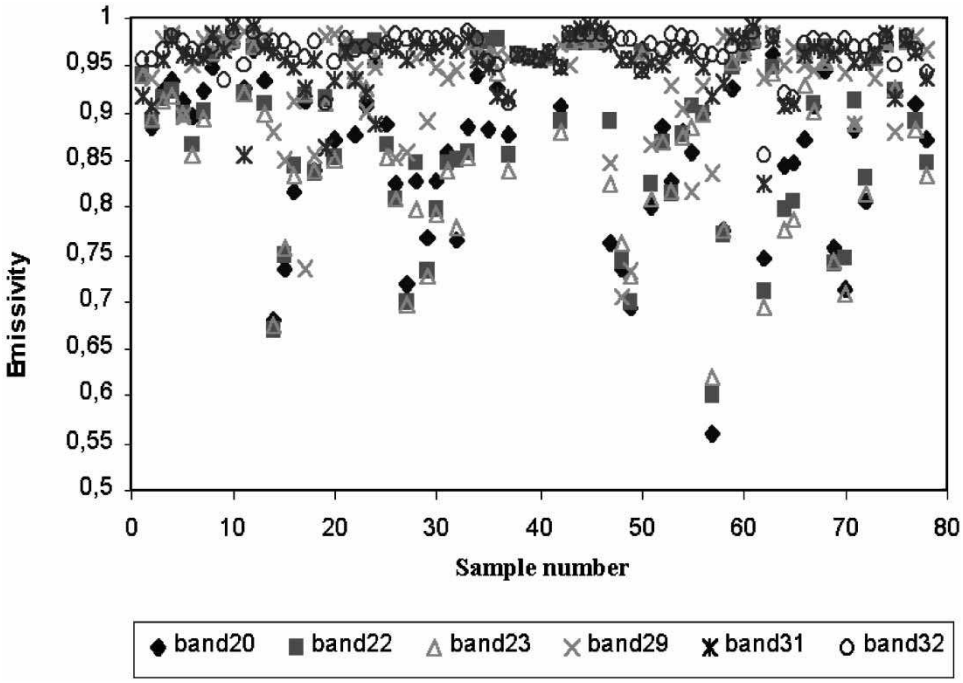

Figure 4. Averaged emissivities of the surfaces considered in the MODIS channels 20, 22, 23, 29, 31 and 32.

and $T+20$ K) (T is the first boundary layer temperature of the atmosphere), and 15 different values of emissivity (ε_i) (see table 2 and figure 4).

2.3. *Algorithms*

In this section, we present some algorithms to retrieve sea and land surface temperature from MODIS data.

2.3.1. *Sea surface temperature*

Three models have been chosen; a linear split window algorithm (SST1), that can be obtained from equation (4) by considering the black body behaviour of the

sea surface (see equation (9)), a linear quadratic algorithm (SST2) obtained from Sobrino and Raissouni (2000) (see equation (10)), and finally a linear algorithm with coefficient dependence on water vapour content (SST3) obtained according to Sobrino *et al.* (1994) (see equation (11)),

$$T_{SST1} = T_{31} + a_0(T_{31} - T_{32}) + a_1 \tag{9}$$

$$T_{SST2} = T_{31} + a_0(T_{31} - T_{32}) + a_1(T_{31} - T_{32})^2 + a_2 \tag{10}$$

$$T_{SST3} = T_{31} + (a_0 + a_1 W)(T_{31} - T_{32}) + a_2 W + a_3 \tag{11}$$

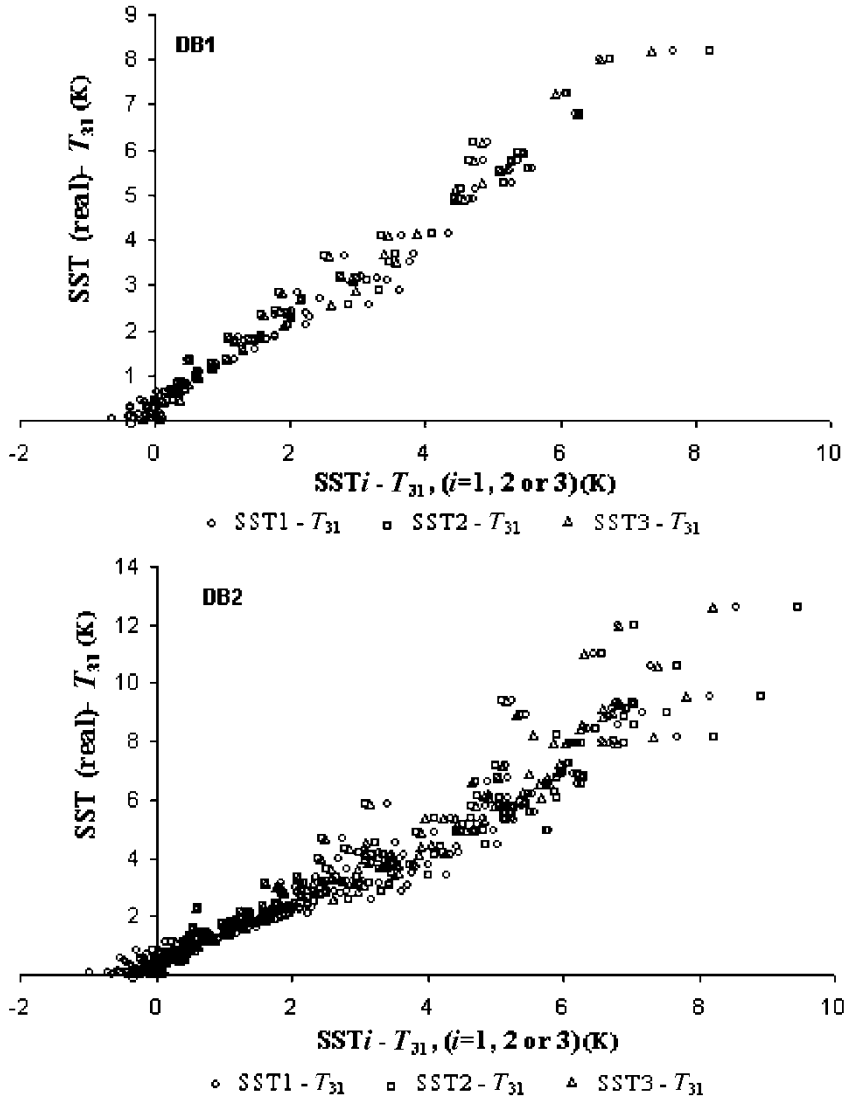

Figure 5. Plot of the temperature difference between the real sea surface temperature (SST) and T_{31} versus the temperature difference between the SST obtained for each algorithm (SSTi) and T_{31}.

where T_{SST1}, T_{SST2} and T_{SST3} are sea surface temperatures obtained for the mentioned algorithms (see figure 5), W is the total amount of atmospheric water vapour and T_{31} and T_{32} are the brightness temperatures in MODIS channels 31 and 32. These two channels are similar to AVHRR channels 4 and 5, and ATSR-2 channels 2 and 1.

In order to obtain the numerical values of the coefficients, simulations made at T, $T-5$ and $T+5$ K, and emissivity values of 0.99 and 0.98 for MODIS channels 31 and 32, respectively were considered. The results of using the least squares minimization procedure are shown in table 3. This table includes the atmospheric residual error, σ_{mod}, the errors introduced by noise during the measurement σ_{Noise}, the errors due to emissivity (σ_{ε}), and water vapour content (σ_W) and finally the total error (σ_{Total}). To evaluate these errors we have assumed a noise equivalent temperature difference (NEΔT) of 0.05 K for MODIS channels 31 and 32, a water vapour content uncertainty of 0.5 g cm^{-2} and an emissivity uncertainty of 0.005. From simulation with DB1, we have estimated the coefficients of the different split window algorithms. In order to check the fitted coefficients for the three models considered, we have used DB2 radiosonde database. σ^*_{Total} indicates the total error obtained when we use the split window coefficients estimated by DB1 and the brightness temperatures simulated by means of MODTRAN 3.5 considering DB2.

2.3.2. *Land surface temperature*

Analogously to the sea case, three models have been considered for LST estimation using MODIS channels 31 and 32 data; a quadratic algorithm (LST1) developed by Sobrino and Raissouni (2000) (see equation (12)), a linear algorithm (LST2) obtained from Sobrino *et al.* (1996) (see equation (13)), and finally, an algorithm (LST3) that follows the structure given by Becker and Li (1990) (see

Table 3. Coefficients of the SST algorithms proposed for MODIS instrument. The last six lines represent respectively the error of each model (σ_{mod}), the same error obtained with DB2 (σ^*_{mod}), the error due to noise (σ_{Noise}), the error due to water vapour uncertainty (σ_W), the total error (σ_{Total}) and the total error obtained with DB2 (σ^*_{Total}). The values have been obtained considering a water vapour content of 1 g cm^{-2}, and $T_{31}-T_{32}=1$ K for dry conditions and 3 g cm^{-2}, 2 K for wet conditions.

Coefficient	SST1	SST2	SST3
a_0	3.83	2.75	1.90
a_1	0.14	0.67	0.44
a_2	–	0.36	0.05
a_3	–	–	0.34
σ_{mod} (K)	0.39	0.34	0.24
σ^*_{mod} (K)	0.45	0.44	0.39
σ_{Noise} (K)	0.31	0.42	0.27
σ_W (K)	–	–	0.47
σ_{Total} (K)	0.50	0.54	0.59
σ^*_{Total} (K)	0.55	0.61	0.67

equation (14)).

$$T_{LST1} = T_{31} + a_1 + a_2(T_{31} - T_{32}) + a_3(T_{31} - T_{32})^2 + (a_4 + a_5 W)(1-\varepsilon) + (a_6 + a_7 W)\Delta\varepsilon \quad (12)$$

$$T_{LST2} = T_{31} + (a_1 + a_2 W)(T_{31} - T_{32}) + a_3 + a_4 W + (a_5 + a_6 W)(1-\varepsilon) + (a_7 + a_8 W)\Delta\varepsilon \quad (13)$$

$$T_{LST3} = a_1 + a_2 W + \left[a_3 + a_4 W + (a_5 + a_6 W)\left(\frac{1-\varepsilon}{\varepsilon}\right) + (a_7 + a_8 W)\frac{\Delta\varepsilon}{\varepsilon^2}\right]\left(\frac{T_{31} + T_{32}}{2}\right) + \left[a_9 + a_{10} W + (a_{11} + a_{12} W)\left(\frac{1-\varepsilon}{\varepsilon}\right) + (a_{13} + a_{14} W)\frac{\Delta\varepsilon}{\varepsilon^2}\right]\left(\frac{T_{31} - T_{32}}{2}\right) \quad (14)$$

where ε [$\varepsilon = (\varepsilon_{31} + \varepsilon_{32})/2$] is the mean effective emissivity in MODIS channels 31 and 32, and $\Delta\varepsilon$ ($\Delta\varepsilon = \varepsilon_{31} - \varepsilon_{32}$) is the spectral emissivity difference, and a_i are the split window coefficients that have been obtained by simulations.

Table 4 shows the numerical values of the split window coefficients given by equations (12) to (14), as well as the estimation errors and the total errors obtained by both the DB1 and DB2 ($\sigma_{total} = \sqrt{\sigma^2_{mod} + \sigma^2_{\varepsilon} + \sigma^2_{W} + \sigma^2_{Noise}}$). In this case, the error due to emissivity uncertainty has been also considered ($\sigma_{\varepsilon} = 0.005$). The coefficients have been obtained for 15 different emissivities extracted from Salisbury spectra database (Salisbury and D'Aria 1992). These emissivities have been previously filtered with the appropriate MODIS channel filter functions (see figure 4). ε_i (with $i = 31$, 32) varying from 0.95 to 1.00, and its spectral variations, $\Delta\varepsilon = \varepsilon_{31} - \varepsilon_{32}$,

Table 4. Coefficients for MODIS LST algorithms, see equations (12), (13) and (14). The last seven lines are respectively the error of the model (σ_{mod}), the same error obtained with DB2 (σ^*_{mod}), the error due to noise (σ_{Noise}), the error associated with the uncertainty in emissivity (σ_{ε}), the error associated with water vapour content (σ_W), the total error (σ_{Total}) and the total error obtained with DB2 (σ^*_{Total}).

Coefficient	LST1	LST2	LST3
a_1	1.02	3.29	0.97
a_2	1.79	−0.12	0.13
a_3	1.20	1.11	1.00
a_4	34.83	−0.04	0.00
a_5	−0.68	38.72	0.112
a_6	−73.27	1.23	0.006
a_7	−5.19	−100.22	−0.52
a_8	–	1.20	0.02
a_9	–	–	9.98
a_{10}	–	–	−0.32
a_{11}	–	–	−36.15
a_{12}	–	–	−0.42
a_{13}	–	–	130.8
a_{14}	–	–	−10.72
σ_{mod} (K)	0.73	1.00	0.88
σ^*_{mod} (K)	1.38	1.53	1.51
σ_{Noise} (K)	0.50	0.25	0.38
σ_{ε} (K)	0.64	0.70	0.28
σ_W (K)	0.03	0.13	0.11
σ_{Total} (K)	1.09	1.25	1.00
σ^*_{Total} (K)	1.60	1.71	1.59

varying from −0.02 to 0.02, with five surface temperatures: $T-5$, T, $T+5$, $T+10$, and $T+20$ K. The table shows also the total error obtained with DB2 (σ^*_{Total}).

2.3.3. *Application to actual data*

A validation of the LST product in wet conditions has been carried out using datasets kindly provided by Zhengming Wan, collected from a field campaign carried out in the low Mississippi River basin late June–August 2002. Five radiometers were deployed in a soybean field. The validation results are given in table 5. Note that the LST1 is the best algorithm with a root mean square error of 0.48 K. Surface and spectral difference emissivity values of: $\varepsilon_{31}=0.99$, $\varepsilon_{32}=0.99$ and $\Delta\varepsilon=0$, have been considered, which are suitable for a soybean field.

3. Atmospheric water vapour content retrieval

Water vapour is widely recognized to be a key climate variable. Indeed it is the principal contributor to the greenhouse effect and plays a key role in our understanding of the Earth's climate. Knowledge of the total atmospheric water vapour content is necessary to improve the precision of the estimates of LST obtained from satellite data by means of split window algorithms. One way to obtain it consists of using radiosonde observations. However, this is not always possible, especially in the case of historical satellite databases. Also, in numerous areas of our planet, mainly in dry areas, radiosonde observations are not carried out in a systematic way, and present infrared sounders (Susskind *et al.* 1984) are capable of retrieving water vapour profiles, but the derived water vapour depends on the initial guess of the meteorological parameters, with greatest dependence close to the surface. To overcome this inconvenience, numerous methods that allow us to estimate the total atmospheric water vapour content have been developed in recent years using data given by sensors, such as the Advanced Very High Resolution Radiometer (AVHRR) (Sobrino *et al.* 1999), and MODIS (Gao and Goetz 1990, Kaufman and Gao 1992). A good method should satisfy the following requirements: (1) low sensibility to the noise due to the statistical errors of the channels, (2) low sensibility to the variability of the other components of the atmosphere, and (3) low sensibility to the variability of the characteristics of the surfaces. In order to take these requirements into account the ratio technique was selected.

3.1. *Ratio technique*

The ratio technique consists of detecting the attenuation that reflected solar radiation suffers due to water vapour absorption after it has transferred down to the surface and back up through the atmosphere. This technique is based on the differential absorption method, which assumes that the transmission in one water vapour absorption channel can be estimated through the ratio of the measured radiances in the absorption channel and at least one window channel. The transmission is then related to the water vapour content. The method and some applications are described and validated in Frouin *et al.* (1989), Gao *et al.* (1993), Bartsch and Fischer (1997); Bouffiès *et al.* (1997). So, the total vertical amount of water vapour can be derived from a comparison between the reflected solar radiation in near infrared non-absorption channels. In order to derive column water

Table 5. Comparison between the algorithms LST1, LST2 and LST3 and *in situ* measured LSTs in validation field campaigns conducted in a soybean field (33.08263° N, 90.7866° W), Mississippi, in 2002 (Wan, personal communication). The atmospheric column water vapour (cwv) comes from MOD07_L2.

Case no.	Granule ID	Date and time (month/day hh:mm)	View zenith (°)	Atmos-pheric cwv (cm)	T_{31} (K)	T_{32} (K)	*In situ* T_s from radiometers (K)	LST1– *in situ* T_s (K)	LST2– *in situ* T_s (K)	LST3– *in situ* T_s (K)
1	A2002199.0415	7/17 23:16 CDT	6.99	3.5	295.2	294.8	296.8	0.5	0.8	1.3
2	A2002215.0415	8/02 23:16 CDT	6.62	3.3	296.2	295.8	298.3	0.3	0.6	1.1
3	A2002217.0400	8/04 23:04 CDT	18.17	3.0	294.8	294.2	297.6	0.0	0.3	0.9
4	A2002220.0430	8/07 23:35 CDT	38.85	3.5	292.4	292.0	294.5	0.0	0.3	0.7
5	A2002222.0420	8/09 23:22 CDT	18.68	3.3	293.0	292.7	295.7	−0.8	−0.5	−0.1

vapour from measurements of solar radiation reflected by the surface, the absorption and scattering properties of the atmosphere and the surface near 1 μm must be taken into account. The radiance at a downward-looking satellite sensor can be written in a simplified form, as (Hansen and Travis 1974, Fraser and Kaufman 1985),

$$L_{\text{Sensor}}(\lambda) = L_{\text{Sun}}(\lambda)\tau(\lambda)\rho(\lambda) + L_{\text{Path}}(\lambda) \tag{15}$$

where λ is the wavelength, $L_{\text{Sensor}}(\lambda)$ is the radiance at the sensor, $L_{\text{Sun}}(\lambda)$ is the solar radiance above the atmosphere, $\tau(\lambda)$ is the total atmospheric transmittance, which is equal to the product of the atmosphere transmittance from the Sun to the Earth's surface and that from the surface to the satellite sensor, $\rho(\lambda)$ is the surface bi-directional reflectance, and $L_{\text{Path}}(\lambda)$ is the path scattered radiance that we assume can be treated approximately as an unspecified fraction of direct reflected solar radiation when the aerosol concentrations are low (Kaufman and Gao 1992). This assumption allows the derivation of column water vapour amounts from satellite data without the need to model single and multiple scattering effects. The feedback effect was neglected because aerosol optical thickness are typically small in the near-IR region. The first term on the right hand side of equation (15) is the direct reflected solar radiation. L_{Direct} is used to represent this component. $L_{\text{Sensor}}(\lambda)/L_{\text{Sun}}(\lambda)$ is defined as the apparent reflectance.

The reflected solar radiation in the absorption band, without the water vapour effect, has to be estimated from the nearby channels. The main uncertainties in this method are the spectral characteristics of the surface in the near IR. Table 6 shows the spectral characteristics of MODIS near IR channels used in this paper to derive the total atmospheric water vapour amount.

The development and simulation of the ratios technique are based on surface reflectance. For some surface covers the reflectance varies almost linearly with wavelength and for this type of cover the best technique is based on linear interpolation of the surface reflectance between two channels around the water absorption channel. We cannot get the water vapour transmittances (see equation (15)) from radiances of individual absorption channels. However, if the surface reflectances are constant with wavelength, a 2-channel ratio of an absorption channel with a window channel gives the water vapour transmittance of the absorption channel. The ratio technique using 2-channels was applied in this paper to derive atmospheric transmittances of the absorption channels, and subsequently the total atmospheric water vapour content. The ratios will be calculated from radiances of MODIS channels 2, 5, 17, 18, and 19 centred at 0.865, 1.24, 0.905, 0.936 and 0.94 μm, respectively. These channel ratios are approximately equal to the atmospheric water vapour transmittances in the Sun-surface-sensor

Table 6. Spectral characteristics of MODIS near IR channels used in water vapour retrieval algorithms.

Band number	Band centre (μm)	Bandwidth (μm)
2	0.865	0.04
5	1.24	0.02
17	0.905	0.03
18	0.936	0.01
19	0.94	0.05

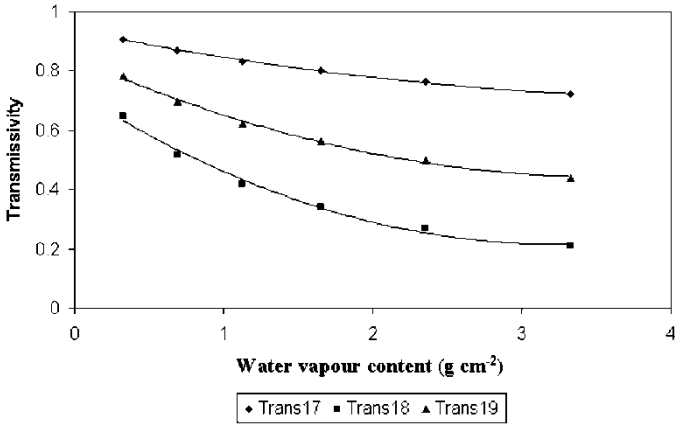

Figure 6. Transmissivity in MODIS channels 17, 18 and 19 versus the total atmospheric water vapour content.

Table 7. Surface reflectance values and ratio $\rho_{0.865}/\rho_{0.94}$ for different surfaces extracted from Salisbury and D'Aria (1992).

Surface	$\rho_{0.865}$	$\rho_{1.24}$	$\rho_{0.905}$	$\rho_{0.936}$	$\rho_{0.94}$	$\rho_{0.865}/\rho_{0.94}$
0015	0.81	0.68	0.79	0.79	0.78	1.03
86p4603	0.22	0.35	0.23	0.25	0.25	0.87
87p313	0.20	0.30	0.21	0.22	0.22	0.91
87p325	0.23	0.31	0.24	0.24	0.24	0.93
87p4264	0.32	0.43	0.34	0.35	0.35	0.90
87p707	0.34	0.42	0.35	0.36	0.36	0.95
89p1793	0.36	0.42	0.36	0.36	0.36	0.98
Conifers	0.52	0.44	0.51	0.51	0.50	1.03
Deciduous	0.55	0.51	0.55	0.55	0.55	1.01
Drygrass	0.57	0.67	0.60	0.62	0.61	0.93
Gneissh1	0.73	0.80	0.73	0.73	0.73	0.99
Granith1	0.16	0.15	0.16	0.16	0.16	1.01
Grass	0.50	0.49	0.51	0.51	0.51	0.98
Limesth1	0.41	0.50	0.41	0.42	0.42	0.98
Marbleh1	0.33	0.31	0.33	0.32	0.32	1.04
Sandsth1	0.49	0.59	0.50	0.51	0.51	0.97
Schisth1	0.25	0.34	0.25	0.25	0.25	1.02
Shaleh1	0.27	0.30	0.27	0.28	0.28	0.98
Siltsth1	0.29	0.28	0.28	0.29	0.29	1.00
Slateh1	0.17	0.17	0.17	0.17	0.17	1.01
Mean	–	–	–	–	–	0.97
Standard deviation	–	–	–	–	–	0.047

ray path (Kaufman and Gao 1992; Gao and Goetz 1990) The values of 2-channel ratios and total atmospheric water vapour content were generated using MODTRAN 3.5. Figure 6 shows a polynomial relationship between total atmospheric water vapour content and transmissivity. Examples of some reflectance values are tabulated in table 7 together with the reflectance ratio of channels 2 (0.865 μm) and 19 (0.94 μm).

3.2. *Algorithm proposed*

We have defined the following ratios G_{17}, G_{18}, and G_{19} as:

$$G_{17} = \frac{L_{17}}{L_2} \tag{16}$$

$$G_{18} = \frac{L_{18}}{L_2} \tag{17}$$

$$G_{19} = \frac{L_{19}}{L_2} \tag{18}$$

where L_i are radiances obtained by simulation for MODIS channels 2, 17, 18, and 19 with MODTRAN 3.5 using six standard atmospheres and 10 types of surface: fresh snow, forest, farm, desert, ocean, cloud deck, old grass, decayed grass, maple leaf, and burnt grass. The simulated amount of water vapour was varied between 0.3 and 3.3 g cm^{-2}. Figure 7 shows the radiance ratios versus the total water vapour amount, a polynomial behaviour is observed;

$$W_{17} = 26.314 - 54.434G_{17} + 28.449G_{17}^2 \tag{19}$$

$$W_{18} = 5.012 - 23.017G_{18} + 27.884G_{18}^2 \tag{20}$$

$$W_{19} = 9.446 - 26.887G_{19} + 19.914G_{19}^2 \tag{21}$$

where W_{17}, W_{18}, and W_{19} are the water vapour values for MODIS channels 17, 18, and 19, respectively. Atmospheric water vapour has very different absorption coefficients over the bandpasses of MODIS channels 17, 18 and 19. As a result, the three channels have different water vapour sensitivities under the same atmospheric condition. The strong absorption channel 18 is most sensitive under dry conditions, while the weak absorption channel 17 is most sensitive under humid conditions (Kaufman and Gao 1992).

Under a given atmospheric condition, the derived water vapour values from the three channels can be different. A mean water vapour value (W) could be obtained

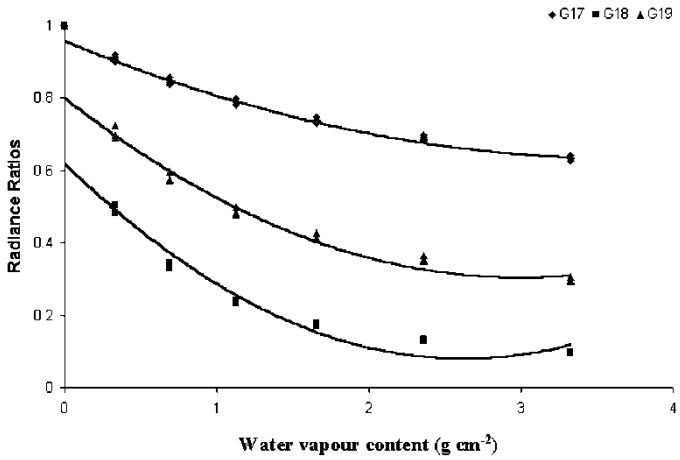

Figure 7. Radiance ratios versus the total atmospheric water vapour amount.

according to the following equation;

$$W = f_{17}W_{17} + f_{18}W_{18} + f_{19}W_{19} \tag{22}$$

where f_{17}, f_{18}, and f_{19} are weighting functions defined according to

$$f_i = \frac{\eta_i}{\sum \eta_i} \tag{23}$$

with $\eta_i = \frac{|\Delta\tau_i|}{|\Delta W|}$, $(i = 17,\ 18,\ 19)$.

Where ΔW is the difference between the maximum and minimum water vapour content from the six standard atmospheres and $\Delta\tau_i$ corresponds to the difference between the transmissivities for the maximum and the minimum water vapour amount obtained in channel (i) (Kaufman and Gao 1992), this expression is justified by the correlation (see figure 6) between the transmissivity and water vapour content.

The values obtained for f_i and η_i are $f_{17} = 0.192$, $f_{18} = 0.453$, $f_{19} = 0.355$, $\eta_{17} = 0.062$, $\eta_{18} = 0.147$ and $\eta_{19} = 0.115$, respectively. So equation (22) can be written as,

$$W = 0.192W_{17} + 0.453W_{18} + 0.355W_{19} \tag{24}$$

Equation (24), is the general method that we proposed to obtain the total water vapour from MODIS images. The advantage of this algorithm is its simplicity as it is derived directly from radiance measurements.

3.3. *Accuracy*

In this section, an analysis of sensitivity has been made. To this end, we apply the error theory to equation (22), according to

$$\sigma_{\text{Total}}(W) = \sqrt{\sum_{i=17}^{19} f_i \Delta W_i^2} \tag{25}$$

where $\Delta W_i = a_i G_i \Delta G_i + b_i \Delta G_i$, with $a_{17} = 56.90$, $a_{18} = 55.77$, $a_{19} = 39.83$, $b_{17} = 54.43$, $b_{18} = 23.02$, and $b_{19} = 26.89$. ΔG_i is obtained according to Kaufman and Gao (1992) as,

$$\Delta G_i = \frac{\sigma\left[G_i\left(3.32\,\text{g cm}^{-2}\right)\right]}{G_i(3.32\,\text{g cm}^{-2}) - G_i(0.33\,\text{g cm}^{-2})} \tag{26}$$

where $\sigma[G]$ is the standard deviation of G for the surface covers considered, and the denominator is the difference between the G_i functions estimated for extreme conditions, humid ($3.32\,\text{g cm}^{-2}$) and dry atmospheres ($0.33\,\text{g cm}^{-2}$). Thus, the sensitivity analysis applied to equation (24) gives a standard deviation of $0.17\,\text{g cm}^{-2}$ for wet atmospheres to $0.06\,\text{g cm}^{-2}$ for dry atmospheres.

3.4. *Evaluation*

In this subsection, a validation of equation (24) is included. To this end, we have used radiosonde observations carried out at 12:00 (GMT) on 29 June, 31 August, 7 September, 9 September, and 14 September 2000. These observations were made at different meteorological stations in Spain (La Coruña, Santander, Gibraltar, Madrid, Murcia, Zaragoza, and Palma de Mallorca) and over Barrax. Figure 8 shows the total atmospheric water vapour content obtained by radiosonde

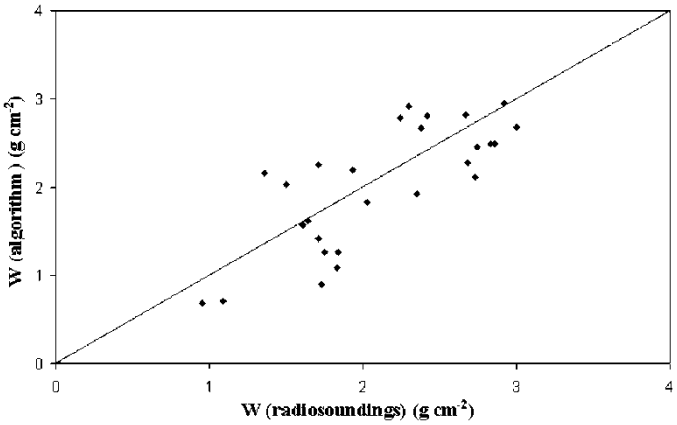

Figure 8. Plot of water vapour content obtained from radiosonde observations versus water vapour content obtained from the proposed algorithm (equation (24)).

observations versus total atmospheric water vapour content obtained by applying the proposed algorithm to the corresponding MODIS images. The results of the comparison give a standard deviation of $0.45\,\mathrm{g\,cm^{-2}}$ and a bias of $0.09\,\mathrm{g\,cm^{-2}}$. This result is similar (a standard deviation of $0.41\,\mathrm{g\,cm^{-2}}$ and a bias of $0.09\,\mathrm{g\,cm^{-2}}$) to the obtained, considering the water vapour content product given by NASA (provided to us by Dr Ridgway), and called MOD05_L2.

4. Application

In this section, we include an application of the LST and the total water vapour content algorithms to MODIS images of the Iberian Peninsula. The algorithms were applied to cloud-free pixels. To this end, we have used the threshold technique given by Saunders and Kriebel (1988), ($T_{32\min}=295\,\mathrm{K}$, $\rho_{1\max}=0.31$, and $(\rho_2/\rho_1)_{\min}=1.16$ for the image of 31 August 2000). Previously to obtain LST, it was necessary to estimate surface emissivity. To solve this problem, we have applied the NDVI threshold method (Sobrino *et al.* 2001). This method, originally developed for AVHRR data, has been adapted here to MODIS images. In our case, the NDVI is obtained from MODIS channels 1 (0.645 μm) and 2 (0.859 μm). The application of the threshold method is carried out taking into account the characteristics of the soil present in the pixels, according to the following procedure:

(i) *Mixed pixels*

It is usually the case that the surface at pixel scale in remote sensing is heterogeneous and rough, which corresponds to values of NDVI between 0.2 and 0.5. The mean and spectral difference emissivity for mixed pixels can be obtained for MODIS channels 31 and 32, according to

$$\varepsilon=0.971+0.018P_v \tag{27}$$

$$\Delta\varepsilon=0.006(1-P_v) \tag{28}$$

where P_v is the vegetation proportion that can be derived according to Carlson and Ripley (1997) from an NDVI image using equation (29):

$$P_v = \frac{(\mathrm{NDVI} - \mathrm{NDVI}_{\min})^2}{(\mathrm{NDVI}_{\max} - \mathrm{NDVI}_{\min})^2} \tag{29}$$

(ii) *Pixels covered by vegetation*

The pixels with a value of NDVI higher than 0.5 are considered as fully

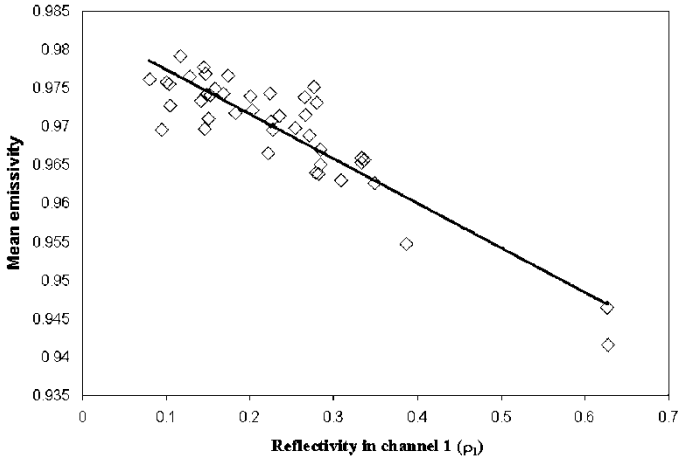

Figure 9. Plot of mean effective emissivity versus surface reflectivity for MODIS channel 1 ($y = -0.0579\ x + 0.9832;\ R^2 = 0.8077$).

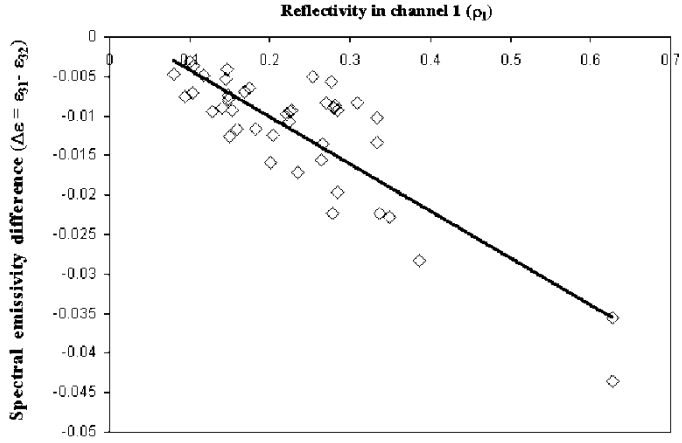

Figure 10. Plot of the spectral emissivity difference versus the reflectivity for MODIS channel 1 ($y = -0.0596\ x + 0.0018;\ R^2 = 0.7066$).

vegetated ($P_v = 1$). Thus, the mean effective emissivity can be written as:

$$\varepsilon = 0.985 + \mathrm{d}\varepsilon \tag{30}$$

with $d\varepsilon = 0.005$.

(iii) *Bare soil pixels*

Values of NDVI lower than 0.2 are considered as soil with sparse vegetation and even bare soil ($P_v = 0$). Using the spectral data of bare soil provided by Salisbury (see figures 9 and 10), for samples whose emissivities in channels 31 and 32 are bigger than or similar to 0.92, two relationships have been obtained by correlating the mean effective emissivity and the channel emissivity difference to the MODIS channel 1 reflectivity (ρ_1) (the reflectivity in channel 1 (ρ_1) was proved to give better correlation than that of channel 2 (ρ_2)), namely

$$\varepsilon = 0.9832 - 0.058\rho_1 \tag{31}$$

$$\Delta\varepsilon = 0.0018 - 0.060\rho_1 \tag{32}$$

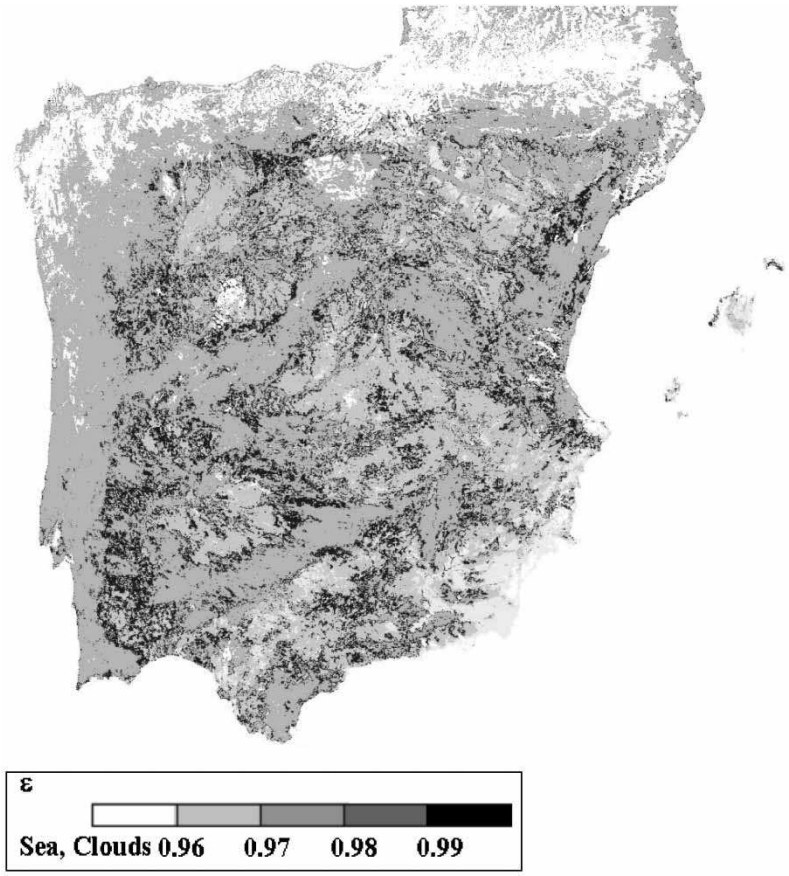

Figure 11. Mean emissivity for 31 August 2000.

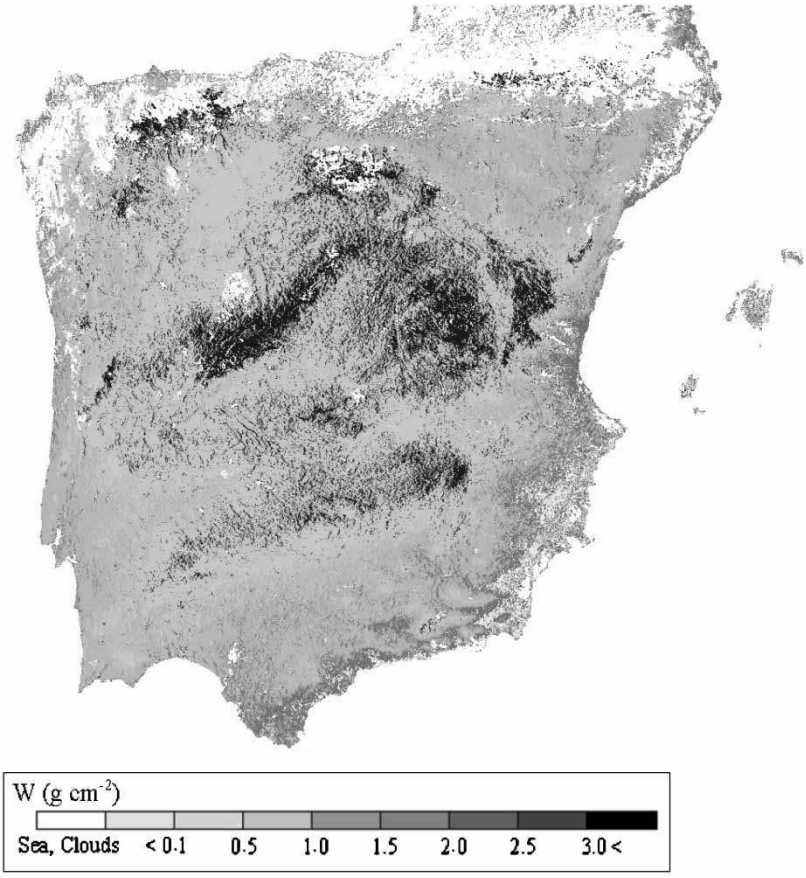

Figure 12. Water vapour content image of the study area for 31 August 2000.

Using this methodology we present in figure 11 the mean emissivity for the MODIS image obtained on 31 August 2000.

Once the total water vapour content (see figure 12) and the emissivity are known, it is possible to apply the LST algorithm given in § 2.3.2 to MODIS images (see figure 13).

5. Conclusions

In this paper, we present operational algorithms to retrieve SST, LST and total atmospheric water vapour from MODIS data. From the simulation, it is shown that sea and land surface temperature can be obtained from MODIS data with an error of 0.3 and 0.7 K, respectively, and the water vapour content can be obtained with a standard deviation lower than $0.2\,g\,cm^{-2}$ from simulation, and an error of $0.4\,g\,cm^{-2}$ from validation with radiosonde observations and MODIS product data. The LST algorithms have been validated using data from the field campaign carried out in the Mississippi, and good results have been obtained.

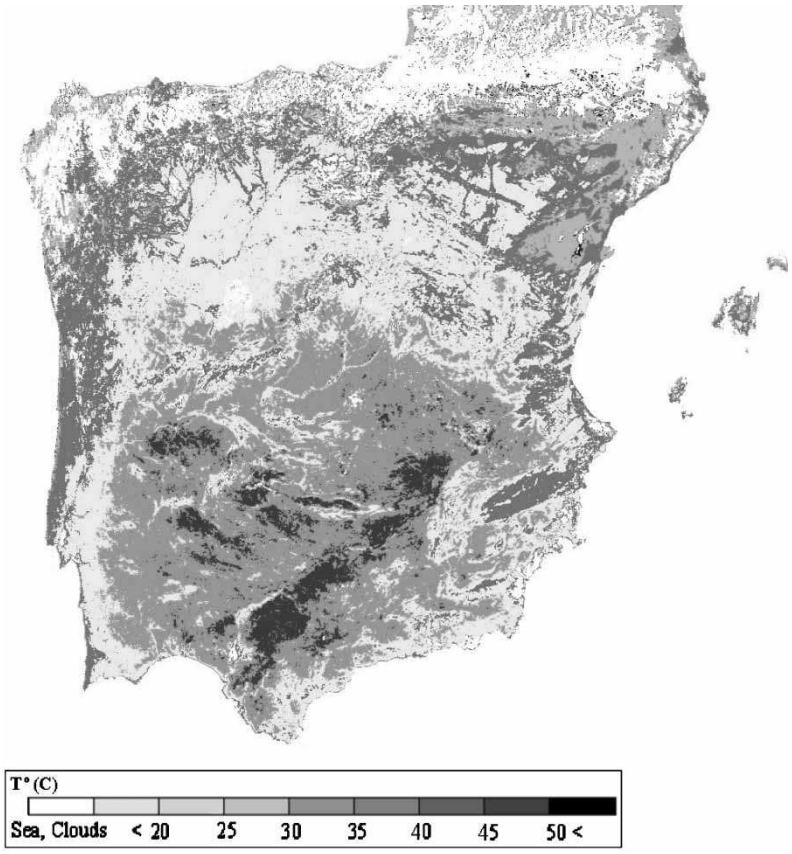

Figure 13. LST1 image obtained for 31 August 2000.

Acknowledgments

We wish to thank Dr Gail Andersson from the Air Force Research Laboratory, Hanscom (USA) for providing us with the MODTRAN 3.5 program, Dr Z. Wan for his useful data and information, Dr B. Gao for his appreciated and constructive comments, Dr Bill Ridgway for providing us with the MODIS images, and the referees of this journal for their appreciated comments. We would also like to thank the European Union for their financial support (WATERMED, Project No. ICA3-ct-1999-00015), and the 'Ministerio de Ciencia y Tecnología' (Project REN2001-3105/CLI). This work has been carried out while Jauad El Kharraz was in receipt of a grant from the WATERMED project.

References

ABREU, L. W., and ANDERSON, G. P., 1996, The MODTRAN 2/3 Report and LOWTRAN 7 Model. Prepared by Ontar Corporation for PL/GPOS, North Andover, MA 01845, USA.

BARTSCH, B., and FISCHER, J., 1997, Passive remote sensing of columnar water vapour content over land surfaces, Max-Planck-Institute of Meteorology report **234**, Hamburg, ISBN 0937-1060.

BECKER, F., and LI, Z.-L., 1990, Towards a local split window method over land surfaces. *International Journal of Remote Sensing*, **11**, 369–394.

BOUFFIÈS, S., BRÉON, F. M., TANRÉ, D., and DUBUISSON, P., 1997, Atmospheric water vapour estimate by a differential absorption technique with the POLDER instrument *Journal of Geophysical Research*, **102**, 3831–3841.

BROWN, O. B., and MINNETT, P. J., 1999, MODIS Infrared Sea Surface Temperature Algorithm Theoretical Basis Document, Version 2.0, http://modis.gsfc.nasa.gov/data/atbd/atbd_mod25.pdf.

CARLSON, T. N., and RIPLEY, D. A., 1997, On the relation between NDVI, Fractional Vegetation Cover, and Leaf Area Index. *Remote Sensing of Environment*, **62**, 241–252.

CASELLES, V., and SOBRINO, J. A., 1989, Determination of frosts in orange groves from NOAA-9 AVHRR data. *Remote Sensing of Environment*, **29**, 135–146.

CHESTERS, D. C., UCCELLINI, L. W., and ROBINSON, W. D., 1983, Low level water vapour fields from the VISSR Atmospheric Sounder (VAS) 'split-window' channels. *Journal of Climatology and Applied Meteorology*, **22**, 725–743.

FRASER, R. S., and KAUFMAN, Y. J., 1985, The relative importance of American soils. *Photogrammic Engineering*, **36**, 955–965.

FROUIN, R., DESCHAMPS, P.-Y., and LECOMTE, P., 1989, Determination from space of atmospheric total water vapour amounts by differential absorption near 940 nm: theory and airborne verification *Journal of Applied Meteorology*, **29**, 448–460.

GAO, B. C., and GOETZ, F. H., 1990, Column atmospheric water vapour and vegetation liquid water retrievals from airborne imaging spectrometer data. *Journal of Geophysical Research*, **95**, 3549–3564.

GAO, B. C., GOETZ, F. H., WESTWATER, E. R., CONEL, J. E., and GREEN, R. O., 1993, Possible near-IR channels for remote sensing of precipitable water vapour from geostationary satellite platforms *Journal of Applied Meteorology*, **32**, 1791–1801.

GUENTHER, B., GODDEN, G. D., XIONG, X., KNIGHT, E. J., QUI, S.-Y., MONTGOMERY, H., HOPKINS, M. M., KHAYAT, M. G., and HAO, Z., 1998, Prelaunch algorithm and data format for the level 1 calibration product for the EOS-AM1 Moderate Resolution Imaging Spectroradiometer (MODIS) *IEEE Transactions on Geoscience and Remote Sensing*, **36**, 1142–1151.

HANSEN, J. E., and TRAVIS, L. D., 1974, Light scattering in planetary atmospheres. *Space Science Reviews*, **16**, 527–610.

KAUFMAN, Y. J., and GAO, B. C., 1992, Remote sensing of water vapour in the near IR from EOS/MODIS. *IEEE Transactions on Geoscience and Remote Sensing*, **30**, 1–27.

KIMURA, F., and SHIMURA, A. P., 1994, Estimation of sensible and latent heat fluxes from soil surface temperature using a linear air land heat transfer model. *Journal of Applied Meteorology*, **33**, 477–489.

KNEIZYS, F. X., SHETTLE, E. P., ABREN, L. W., CHETWYND, J. H., ANDERSON, G. P., GALLERY, W. O., SELBY, J. E. A., and CLOUGH, S. A., 1988, User's guide to LOWTRAN 7. Air Force Geophysics Laboratory, Hanscom AFB, MA 01731 *Environmental Research Papers*, No. 1010.

ROTHMAN, L. S., GAMACHE, R., TIPPING, R., RINSLAND, C., SMITH, M., BENNER, D. C., DEVI, V. M., FLAUD, J.-M., CAMY-PEYRET, C., PERRIN, A., GOLDMAN, A., MASSIE, S., BROWN, L., and TOTH, R., 1992, The HITRAN molecular database: editions of 1991 and 1992. *Journal of Quantitative Spectroscopy and Radiative Transfer*, **48**, 469.

SALISBURY, J. W., and D'ARIA, D. M., 1992, Emissivity of terrestrial materials in the 8–14 μm atmospheric window. *Remote Sensing of Environment*, **42**, 83–106.

SAUNDERS, R. W., and KRIEBEL, K. T., 1988, An improved method for detecting clear sky and cloudy radiances from AVHRR data. *International Journal of Remote Sensing*, **9**, 123–150.

SELLERS, P. J., HALL, F. G., ASRAR, G., STREBEL, D. E., and MURPHY, R. E., 1988, The first ISLSCP Field Experiment (FIFE). *Bulletin of the American Meteorology Society*, **69**, 22–27.

SOBRINO, J. A., and RAISSOUNI, N., 2000, Toward remote sensing methods for land cover dynamic monitoring: application to Morocco. *International Journal of Remote Sensing*, **21**, 353–366.

SOBRINO, J. A., LI, Z-L., STOLL, M. P., and BECKER, F., 1994, Improvements in the split-window technique for the land surface temperature determination. *IEEE Transactions on Geoscience and Remote Sensing*, **32**, 243–253.

SOBRINO, J. A., LI, Z.-L., STOLL, M. P., and BECKER, F., 1996, Multi-channel and multi-angle algorithms for estimating sea and land surface temperature with ATSR data. *International Journal of Remote Sensing*, **17**, 2089–2114.

SOBRINO, J. A., RAISSOUNI, N., SIMARRO, J., NERRY, F., and FRANÇOIS, P., 1999, Atmospheric water vapour content over land surfaces derived from the AVHRR data. Application to the Iberian Peninsula *IEEE Transactions on Geoscience and Remote Sensing*, **37**, 1425–1434.

SOBRINO, J. A., RAISSOUNI, N., and LI, Z-L., 2001, A comparative study of land surface emissivity retrieval from NOAA data. *Remote Sensing of Environment*, **75**, 256–266.

SODEN, B., TJEMKES, S., SCHMETZ, J., SAUNDERS, R., BATES, J., ELLINGSON, B., ENGELEN, R., GARAND, L., JACKSON, D., JEDLOVEC, G., KLEESPIES, T., RANDEL, D., RAYER, P., SALATHE, E., SCHWARZKOPF, D., SCOTT, N., SOHN, B., DE SOUZA-MACHADO, S., STROW, L., TOBIN, D., TURNER, D., VAN DELST, P., and WEHR, T., 2000, An intercomparison of radiation codes for retrieving UTH in the 6.3-μm band: a report from the first GVaP workshop *Bulletin of the American Meteorological Society*, **81**, 797–808.

SUSSKIND, J., ROSENFIELD, J., REUTER, D., and CHAHINE, M. T., 1984, Remote sensing of weather and climate parameterisation HIRS2/MSU on TIROS-N. *Journal of Geophysical Research*, **89**, 4677–4697.

VINING, R. C., and BLAD, B. L., 1992, Estimation of sensible heat flux from remotely sensed canopy temperatures. *Journal of Geophysical Research*, **97**, 18951–18954.

WAN, Z., 2002, Estimate of noise and systematic error in early thermal infrared data of the Moderate Resolution Imaging Spectroradiometer (MODIS). *Remote Sensing of Environment*, **80**, 47–54.

WAN, Z., and DOZIER, J., 1996, A generalized split-window algorithm for retrieving land-surface temperature from space. *IEEE Transactions on Geoscience and Remote Sensing*, **34**, 892–905.

WAN, Z., and LI, Z.-L., 1997, A physics-based algorithm for retrieving land-surface emissivity and temperature from EOS/MODIS data. *IEEE Transactions on Geoscience and Remote Sensing*, **35**, 980–996.

WATTS, P. D., ALLEN, M. R., and NIGHTINGALE, T. J., 1996, Wind speed effects on sea surface emission and reflection for the Along Track Scanning Radiometer. *Journal of Atmospheric and Ocean Technology*, **13**, 126–141.